Article

Accuracy of 3D-Printed Master Cast Workflow Using a Digital Light Processing Printer

Saskia Berndt [1,*], Hannah Herstell [1], Stefan Raith [2], Christina Kühne [1] and Sven Reich [1]

1 Department of Prosthodontics and Biomaterials, RWTH Aachen University Hospital, Pauwelsstrasse 30, 52074 Aachen, Germany; hannah.herstell@rwth-aachen.de (H.H.); chkuehne@ukaachen.de (C.K.); sreich@ukaachen.de (S.R.)
2 Department of Oral and Maxillofacial Surgery, RWTH Aachen University Hospital, Pauwelsstrasse 30, 52074 Aachen, Germany; sraith@ukaachen.de
* Correspondence: saskia.berndt@rwth-aachen.de

Abstract: This in vitro study was designed to investigate whether conventionally produced casts and printed casts for prosthodontic purposes show comparable full-arch accuracy; a ceramic reference cast with inlay and crown preparations was fabricated. Ten gypsum casts were fabricated from conventional silicone elastomeric impressions. Ten digital impressions [IOS] of the reference cast were obtained by an intraoral scanner to fabricate 3D-printed resin casts. The ceramic reference cast, the gypsum, and the printed casts were digitized by an industrial structured light scanner (ILS) and provided as stl files. To evaluate absolute mean trueness values, the digitized gypsum casts [CON], digitized printed casts [PRINT], and [IOS] were superimposed with the digitized ceramic reference cast [REF]. Additionally, each [IOS] scan was compared with its corresponding [PRINT]. The precision was calculated for [CON], [IOS], and [PRINT]. The Mann–Whitney U test for independent samples and the Wilcoxon test for connected samples were performed ($p \leq 0.05$). As absolute mean deviation trueness values were obtained: 69 ± 24 μm for [REF]-[CON], 33 ± 4 μm for [REF]-[PRINT], and 19 ± 3 μm for [REF]-[IOS]. The superimposition [IOS]-[PRINT] revealed 38 ± 6 μm. The precision was 74 ± 22 μm for [CON], 32 ± 10 μm for [PRINT], and 15 ± 4 μm for [IOS]. With respect to the workflow, the trueness values of [REF]-[CON] and [REF]-[PRINT] differed significantly. Within the digital workflow, [REF]-[PRINT], [REF]-[IOS], and [IOS]-[PRINT], all values differed significantly. Within the limitations of the study, digital impression and printed cast fabrication were more accurate and reproducible than the conventional workflow.

Keywords: additive manufacturing; digital light processing; dental; cast; 3D-printing; accuracy; trueness; precision; intraoral scan (IOS)

1. Introduction

If comprehensive fixed prosthetic rehabilitations are manufactured based on intraoral optical impressions, there are several reasons for the necessity to produce real casts. To save time during try-in of dental restoration at the patient, multiple proximal and occlusal contacts can be checked extraorally on real casts which might reduce the overall intraoral adaptation time. Real casts facilitate visualizing, checking, and modifying the static and dynamic occlusion in the dental technician laboratory. If an individual veneering of a metal-based or ceramic framework is necessary, the availability of a real cast is mandatory, too [1]. For all described purposes, the full-arch accuracy is required.

To produce real casts from a data set of an intraoral optical impression, subtractive or additive methods are applied. Whereas subtractive methods such as milling are of minor relevance, 3D printing technology is a common method to transfer virtual 3D information into reality. In dentistry, the following technologies can be distinguished: stereolithography (SLA), digital light processing (DLP), and continuous liquid interface production (CLIP) as vat polymerization technologies, fused filament fabrication (FFF) in

material extrusion, material jetting (MJ), and binder jetting (BJ) technologies as well as powder bed fusion technologies such as selective laser sintering or melting (SLS/M) [2,3]. In vat polymerization, a photosensitive resin is polymerized layer by layer with light [4,5]. DLP, as used in this study, cures one layer at a time using a light source, such as light-emitting diodes, covering wavelength ranges from deep ultraviolet to visible [5,6]. SLA, on the other hand, cures one layer point by point using a coherent light source (usually an ultraviolet (UV) laser beam). CLIP differs from the other vat polymerization techniques in its oxygen-permeable membrane to inhibit radical polymerization at the surface close to the UV source [2,5]. Material extrusion describes a technique in which thermoplastic materials are melted and extruded through a jet head forming objects by filament layering [7]. Jetting technologies extrude either a liquid photosensitive resin (material jetting) which is polymerized with UV light or a binder (binder jetting) [4,8]. Binder jetting uses bonding agents to fuse powders. Selective laser sintering and melting work with a laser to sinter or melt and then fuse powdered materials such as polymers, metal, ceramic, or glass, which are applied layer-by-layer via rollers [3,9].

The advantages of additive manufacturing are less material waste and nearly unlimited degrees of freedom in manufacturing compared to subtractive methods [1]. At the same time, it allows unlimited replica production and provides a wide range of indications such as the production of casts, surgical guides, occlusal splints, and temporary restorations [4,10]. Printed resin casts show fewer abrasion, less fracture risk, and light weight [11]. Apart from that, model editing is virtually facilitated and quick data transfer to a dental laboratory or other practitioners is possible [12].

Printed casts are a feasible alternative for conventional gypsum casts regarding trueness and precision. However, the staircase effect is undeniable due to the layer-by-layer approach of vat polymerization methods. There are two main causes for this effect, one of them being the geometric approximation of a curved surface by layers with uniform thickness and the second one being material shrinkage of each individual layer while printing [13]. For staircase control, layer thickness should be decreased [13]. Staircases were reported to cause a dimensional error and poor surface roughness resulting in additively manufactured objects unacceptable for many indications [14]. For tasks such as waxing, printed casts are not necessarily usable.

For 3D printing, the environmental impact, printing time, and cost are other important topics in comparison with conventional manufacturing. Environmental factors such as resource consumption, material waste, and energy consumption either by the 3D manufacturing process itself or due to disposal cannot be neglected [15]. Next to energy consumption, costs are influenced by the acquisition cost of the printer solution and running costs for resin, gas, and isopropyl alcohol. Printing time can be reduced by the orientation of the object on the building platform. Horizontally oriented parts require reduced printing time compared to vertically oriented parts. A higher layer thickness results in reduced printing time, too, but impairs surface quality [16]. If it is necessary to obtain a real cast from an intraoral digital impression for a prosthodontic work, the accuracy of the fabrication process is crucial. Accuracy is defined by the subterms trueness and precision [17]. For trueness evaluation, a test object, which represents a copy of the original object is compared with this original object to evaluate deviations between the test object and the original [17,18]. Precision defines the reproducibility [17]. For precision analysis test objects (copies) from the same original reference, objects are produced with the same device and method [17]. These copies are compared with each other [17,18].

In digital dentistry, distance measurements or 3D surface comparisons can be accomplished to compare test and original objects [2]. To enable virtual 3D surface measurements, it is necessary to digitize real objects with a high-resolution industrial scanner. For jaw-sized scans, industrial scanners, such as the ATOS III Triple Scan, have a trueness of 3 μm and precision of 2 μm [19]. Once all objects are converted into 3D data, they can be superimposed by a registration process. During the registration process, the data sets are aligned as close as possible in one coordinate system. Applying a best-fit algorithm, even

supposedly identical data sets show deviations meaning that the surface of one data set can be partly located relatively above the other and in some areas below. Therefore, from the measurement direction of one data set, values of <0, 0, and >0 are obtained in relation to the aligned data set. In conclusion, the output of the deviation values has to be differentiated between minus or plus values or the values have to be processed as absolute numbers.

Three-dimensional evaluations can focus on specific areas of interest like full-arch accuracy, interproximal areas, occlusal surfaces, or preparation margins. In the present study, the full-arch accuracy and local accuracy of casts obtained by a conventional and a digital workflow were investigated. In the conventional workflow, silicone impressions were applied to produce gypsum casts. In the digital workflow, intraoral optical impressions were used to generate data for 3D printing. The null hypothesis was that the cast obtained from the conventional and digital workflow did not differ significantly at $p \leq 0.05$. Additionally, the deviations within the digital workflow were evaluated. Therefore, the deviations between the reference cast and digital intraoral impression and the differences between digital intraoral impression and the printed cast were analyzed.

For the local accuracy of the preparations which were integrated into the cast, the null hypothesis stated that there were no statistically significant differences between the digital and conventional workflow.

2. Materials and Methods

Preparation of a Reference Cast

As described by Yatmaz et al. [20], a maxillary reference cast was produced (Figure 1):

Figure 1. Reference cast with an yttrium-stabilized zirconium oxide base and lithium disilicate glass-ceramic teeth; prepared surfaces of the teeth were non-glazed.

Initially, selected teeth of a maxillary typodont (Basic Study Model, KaVo Dental GmbH, Biberach, Germany), missing the right first molar, were prepared for all-ceramic restorations. The left first premolar was prepared for an inlay, whilst the left first molar, the right first premolar, and the right second molar were prepared for crowns. The typodont model was digitized by an intraoral scanner (Cerec Primescan, software v5.1 Dentsply Sirona, Bensheim, Germany) to create a digital cast. Prior to separating the digital cast into an alveolar base and single teeth, the acquired data were extracted as a standard tessellation language (STL) file and uploaded into a 3D software (Blender v2.78, Blender Foundation, Amsterdam, The Netherlands). The base, consisting of yttrium-stabilized zirconium oxide (IPS e.max ZirCAD Prime, A3, Ivoclar Vivadent AG, Schaan, Liechtenstein), was milled using a 5-axis milling machine (Coritec 250i; imes-icore GmbH, Eiterfeld, Germany). The teeth were produced from lithium disilicate glass-ceramic blocks (IPS e.max CAD LT A2, Ivoclar Vivadent AG, Schaan, Liechtenstein) by another milling machine (Cerec MC XL,

Dentsply Sirona, Bensheim, Germany). After milling, the teeth were crystallized (Programat P500, Ivoclar Vivadent AG, Schaan, Liechtenstein) and the coronal parts of the teeth, except for the prepared areas, were glazed (IPS Ivocolor Glaze Paste FLUO and mixing liquid allround, Ivoclar Vivadent AG, Schaan, Liechtenstein). The root segments of the teeth were etched with fluoric acid and silanized (IPS Ceramic Etching Gel and Monobond plus, Ivoclar Vivadent AG, Schaan, Liechtenstein). The sockets of the base were airborne particle abraded with ≤50 μm aluminum oxide at 0.1 MPa. Then, the root segments of the teeth were adhesively cemented into the sockets using a phosphoric acid-containing composite (Panavia 21 Ex, Kuraray Europe GmbH, Hattersheim am Main, Germany).

After applying a scanning spray (Scan Spray Stone, Dentaco GmbH & Co. KG, Essen, Germany), the reference cast was scanned by an industrial structured light scanner (ILS) (GOM ATOS III Triple Scan, topometric GmbH, Göppingen, Germany). The cast was scanned five times to check precision. The scans were provided as standard tessellation language (stl) files. For trueness evaluation, one of the casts was randomly selected.

Conventional Workflow

Cast Preparation and Scan

The interproximal spaces of the reference cast were blocked out with wax. To check for any wax residues on the teeth surfaces a microscope (ZEISS OPMI pico, Carl Zeiss Surgical GmbH) was used. Rim-Lock Trays, size U2 (Orbi-Lock, Orbis Dental), were coated with a universal adhesive (Kulzer GmbH, Hanau, Germany). Single-step two-phase silicone elastomeric impressions were taken. A high-viscosity and low-viscosity material consisting of polyvinyl siloxanes (HEAVY Regular Set DECA and Aquasil Ultra+ XLV Regular Set, Dentsply DeTrey GmbH, Konstanz, Germany) were used. The impressions were removed from the cast after five minutes and disinfected for 10 min (Kanipur, KANIEDENTA, Dentalmedizinische Erzeugnisse GmbH, Herford, Germany) to simulate the clinical workflow. Thirty minutes post disinfection, the impressions were poured with type IV gypsum (20 mL water/100 g gypsum, vacuum mixed for 30 s) (BEGO Stone plus, BEGO, Bremen, Germany) by an experienced technician. The impressions were removed from the gypsum cast after a setting time of 30 min. Under dry conditions, sharp edges of the base were trimmed. A total of ten casts were made and then digitized with an ILS (GOM ATOS Triple Scan, topometric GmbH, Göppingen, Germany).

Digital Workflow

Cast Preparation and Scan

The reference all-ceramic cast was scanned ten times by an intraoral scanner (Primescan, Sirona Dental Systems GmbH, Bensheim, Germany) using the Cerec 5.2.2 RC 1 software. The scanning path described by Passos et al. [13] was applied by one operator in a darkened room. In the acquisition phase, each cast was trimmed so that the teeth and the alveolar ridge representing the keratinized gingiva were kept. In the model phase, the cast was shown after calculation by the scanning software with its base. This solid cast was carved out from the bottom to reduce material. The virtual casts were exported as system-specific 'cam' files and imported into the inLab CAM software (software 22.1 Beta 1, Sirona Dental Systems GmbH, Bensheim, Germany). For the printing device, Primeprint (Sirona Dental Systems GmbH, Bensheim, Germany) was chosen. The support structures were defined, and the printing process was initiated. The default parameters which included the number and position of the support structures with a spherical support tip were confirmed. Optimized quality was selected as an orientation strategy on the building platform. The detail quality "very high" for printing was chosen. For the polymer, a specific resin (Primeprint Model, Sirona Dental Systems GmbH, Bensheim, Germany) was used. Two casts were arranged automatically and printed at the same time. After printing, post processing was performed by the post processing unit (Primeprint PPU, Sirona Dental Systems GmbH, Bensheim, Germany) to remove uncured resin by rinsing the specimens and for final resin polymerization. After completing the job, the support structures were removed. The casts were digitized with the same aforementioned ILS, and the files were provided as stl files. Printing parameters can be found in Table 1.

Table 1. Three-dimensional (3D) printing parameters settings.

Resin	
Flexural strength [MPa]	>70
Elastic modulus [MPa]	>1500
Hardness [Shore D]	>80
Color	sand
Curing wavelength [nm]	385
CAM Settings	
Printer	
DMD projector resolution [pixels]	1920×1024
Spectral maximum of LED	385 nm
Membrane type of material unit	flexible
Support Structures	
Distribution	Based on object geometry
Density	Medium
Size	Medium
Spherical support tip	Yes
Cast	
Orientation strategy	Optimized quality
Detail level (layer thickness [μm])	Very high (50)
Post processing	
Washing solution	99.9% isopropyl alcohol

Available Data Files for Surface Comparison by Superimposition

Five ILS scans of the ceramic reference cast served for the precision analysis of the ILS reference scanner. To analyze the conventional and digital cast fabrication, one randomly selected stl file of the digitized reference cast [REF], the ten stl files of the scanned gypsum casts [CON], and the ten stl files of scanned printed casts [PRINT] were available. Additionally, the ten intraoral scans [IOS] within the digital print workflow were exported as stl files for analysis. All superimpositions were performed in GOM Inspect Suite 2020.

Trueness

For full-arch trueness evaluation the combinations of [REF]-[CON], [REF]-[PRINT], [REF]-[IOS] and [IOS]-[PRINT] were available. For test combinations involving [REF], [REF] was defined as a reference object for surface combination while [CON], [PRINT] and [IOS] were the test objects. According to the definition of trueness testing, only one [REF] data file served as reference and was tested against ten [CON], [PRINT], and [IOS] files each. Unlike the actual definition of trueness testing, within the surface comparisons [IOS]-[PRINT], the [IOS] files were set as reference objects. Each of the ten [IOS] files was superimposed with its corresponding [PRINT] file.

All test objects were superimposed with the reference object in one coordinate system via global best-fit alignment. To avoid the inclusion of outliers, the meshes of all test casts were cut interdentally, and all parts of the gingiva were cut out (Figure 2b).
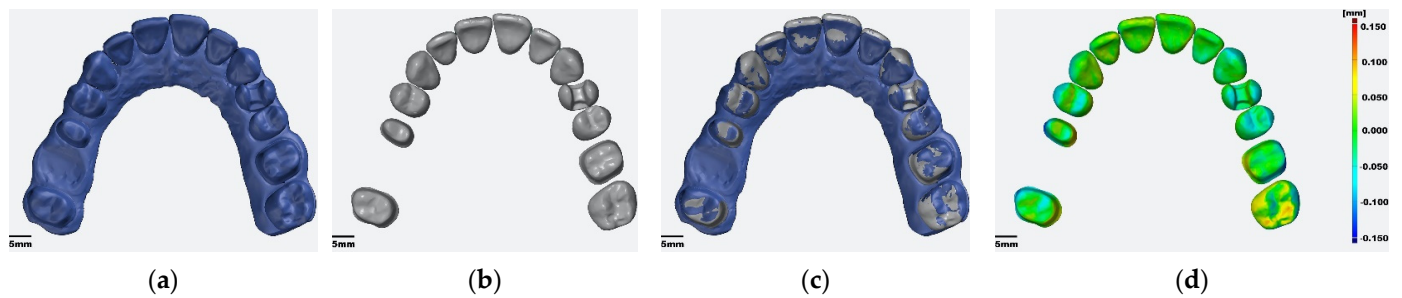
Figure 2. Principle of trimming of all test casts, best-fit alignment, and surface comparison: (**a**) reference cast; (**b**) test cast; (**c**) superimposition of reference and test cast; (**d**) surface comparison [Scale ± 150 μm].

For local trueness evaluation of each preparation type (fixed dental prosthesis (FDP 17-15), inlay (24), and single crown (26)), the preparation surfaces were superimposed with the reference cast via local best-fit alignment (Figure 3). For FDP, only the surface of 17 was set as a reference for local best-fit alignment. [local_CON$_{17-15,24,26}$], [local_PRINT$_{17-15,24,26}$], and [local_IOS$_{17-15,24,26}$] were measured against the reference file.
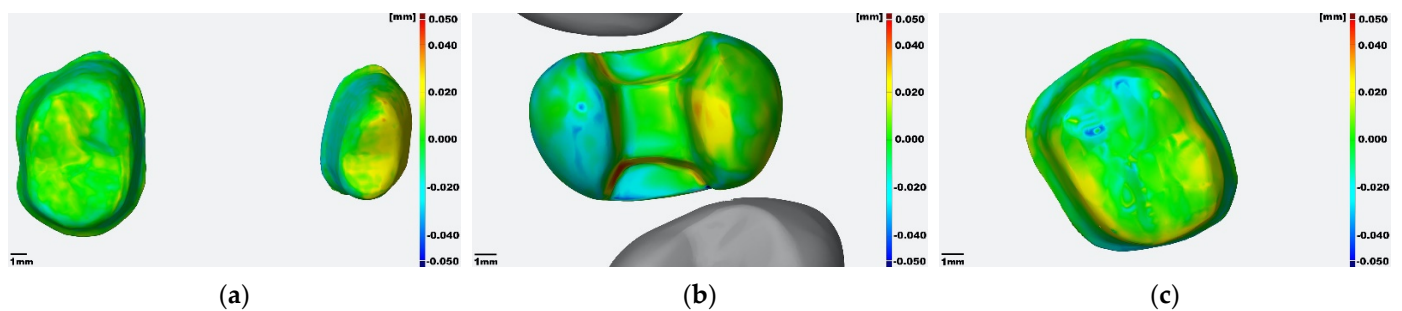

Figure 3. Local trueness evaluation via surface comparison: printed against reference: (**a**) [local_PRINT$_{17-15}$;]; (**b**) [local_PRINT$_{24}$]; (**c**) [local_PRINT$_{26}$] [Scale ± 50 μm].

Before point-to-surface measurement, the maximum tolerance was set to two millimeters and the surface comparison was applied on the test object. The values of the single distance measurements between two surfaces were exported as absolute values in American Standard Code for Information Interchange (ASCII) files.

Each single data set of surface comparison contained approximately 300,000 point-to-surface measurements. For these values, a self-programmed python script for automated data evaluation was developed. This application allowed to run a data analysis under different prerequisites. For descriptive analysis, it was possible to include all deviation measurements or to exclude 1%, 5%, or 10% of the highest and lowest measurement values to avoid non-relevant outliers. In this study, all values were included and the absolute mean deviation, root mean square error (RMSE), median, standard deviation, and minimal and maximal distances were calculated. RMSE is defined as:

$$\text{RMSE} = \sqrt{\frac{1}{n}\sum_{i=1}^{n}(x_i - \mu_i)^2}$$

where x_i are the predicted values of the reference cast, μ_i are the observed values of the test cast, and n is the number of observations. The RMSE describes the dispersion around a true value with respect to trueness and precision.

Precision

To analyze precision, the same alignment and superimposition procedure was applied, comparing the ILS scans of the ten gypsum casts [CON], the ILS scans of ten printed casts [PRINT], and the ten intraoral scans [IOS] among each other leading to 45 surface

comparisons each. The five ILS scans of the reference cast were compared with each other, too, leading to ten comparisons.

Statistics

SPSS 26 (IBM Corporation, Armonk, NY, USA) was used for statistical calculations.

For full-arch trueness, the Shapiro–Wilk test revealed that the data of [REF]-[PRINT] and [REF]-[IOS] were not normally distributed. Therefore, the Mann–Whitney U test (two-tailed) was applied to test whether there was a statistically significant difference between [REF]-[CON] and [REF]-[PRINT] at $p \leq 0.05$. The Wilcoxon test was used (Bonferroni corrected) to check whether there was a significant difference between the trueness data of the related samples [REF]-[IOS], [IOS]-[PRINT] and [REF]-[PRINT] at $p \leq 0.05$.

For the local absolute mean trueness, the Shapiro–Wilk test revealed a non-normal distribution for [local_CON$_{26}$], [local_IOS$_{26}$], and [local_IOS$_{24}$]. For the RMSE trueness, the values of [local_IOS$_{26}$] were not normally distributed. Therefore, the Mann–Whitney U test (two-tailed) was applied to test whether there was a statistically significant difference between the local deviation values between the test casts and the reference cast at $p \leq 0.05$. The Wilcoxon test was used (Bonferroni corrected) to check whether there was a significant difference between the trueness data of the related samples [local_PRINT$_{17\text{-}15,24,26}$] and [local_IOS$_{17\text{-}15,24,26}$] at $p \leq 0.05$.

The precision data of [IOS] were not normally distributed according to the Shapiro–Wilk test. Due to the normal distribution of [CON] and [PRINT], the *t*-test was applied to test for significant differences. [PRINT] and [IOS] were tested for significant differences using the Wilcoxon test.

3. Results

3.1. Full-Arch Trueness

The trueness data of [REF]-[CON], [REF]-[PRINT], [REF]-[IOS], and [IOS]-[PRINT] are displayed in Table 2.

Table 2. Full-arch trueness values.

	N	Absolute Mean Deviation [μm]				RMS Error [μm]			
		Minimum	Maximum	Mean ± Standard Deviation	Median	Minimum	Maximum	Mean ± Standard Deviation	Median
[REF]-[CON]	10	38	105	69 ± 24 [1]	68	78	160	119 ± 29 [1]	105
[REF]-[PRINT]	10	30	44	33 ± 4 [1,2]	33	41	61	48 ± 6 [1,2]	47
[REF]-[IOS]	10	16	25	19 ± 3 [2]	18	42	74	56 ± 10	55
[IOS]-[PRINT]	10	28	49	38 ± 6 [2]	38	45	70	58 ± 7 [2]	59

[1] Statistically significant differences according to the Mann–Whitney U-test. [2] Statistically significant differences according to the Wilcoxon test.

3.1.1. Absolute Mean Deviation

The absolute mean deviation values were 69 μm (SD ± 24 μm) for [REF]-[CON], 33 μm (SD ± 4 μm) for [REF]-[PRINT], 19 μm (SD ± 3 μm) for [REF]-[IOS], and 38 μm (SD ± 6 μm) for [IOS]-[PRINT]. The values of [REF]-[CON] differed significantly from the values of [REF]-[PRINT]. The comparison of [REF]-[PRINT], [REF]-[IOS], and [IOS]-[PRINT] with each other revealed statistically significant differences.

3.1.2. Root Mean Square Error

The RMSE values were 119 μm (SD ± 29 μm) for [REF]-[CON], 48 μm (SD ± 6 μm) for [REF]-[PRINT], 56 μm (SD ± 10 μm) for [REF]-[IOS], and 58 μm (SD ± 7 μm) for [IOS]-[PRINT]. The RMSE values of [REF]-[CON] differed significantly from the values of [REF]-[PRINT]. [IOS]-[PRINT] and [REF]-[PRINT] differed significantly.

3.2. Local Trueness

The trueness data of [local_CON], [local_PRINT], [local_IOS] for the FDP (17-15), the inlay (24), and the single crown (26) preparation are displayed in Table 3. The absolute mean and RMSE values of [local_CON$_{24}$] and [local_CON$_{26}$] differed significantly from the corresponding values of [local_PRINT$_{24}$] and [local_PRINT$_{26}$]. Within the print workflow, the comparisons of absolute mean and RMSE values between [local_PRINT$_{17-15}$] and [local_IOS$_{17-15}$] and between [local_PRINT$_{24}$] and [local_IOS$_{24}$] showed statistically significant differences.

Table 3. Local Trueness values.

	Absolute Mean Deviation [μm] Mean ± Standard Deviation			RMS Error [μm] Mean ± Standard Deviation		
	FDP 17-15	Inlay 24	Crown 26	FDP 17-15	Inlay 24	Crown 26
[local_CON]	31 ± 11	38 ± 13 [1]	61 ± 33 [1]	53 ± 23	86 ± 26 [1]	85 ± 38 [1]
[local_PRINT]	26 ± 7 [2]	14 ± 2 [1,2]	14 ± 5 [1]	35 ± 9 [2]	19 ± 3 [1,2]	18 ± 5 [1]
[local_IOS]	11 ± 2 [2]	10 ± 1 [2]	7 ± 6	15 ± 4 [2]	12 ± 2 [2]	9 ± 7

[1] Statistically significant differences according to the Mann–Whitney U test. [2] Statistically significant differences according to the Wilcoxon test.

3.3. Precision

The precision data of [CON], [PRINT], and [IOS] are shown in Table 4.

Table 4. Precision values.

	N	Precision Based on Absolute Mean Deviation [μm]				Precision Based on RMS Error [μm]			
		Minimum	Maximum	Mean ± Standard Deviation	Median	Minimum	Maximum	Mean ± Standard Deviation	Median
[CON]	10	28	120	74 ± 22 [1]	74	68	184	130 ± 26 [1]	128
[PRINT]	10	11	59	32 ± 10 [1,2]	32	40	101	66 ± 12 [1,2]	65
[IOS]	10	10	27	15 ± 4 [2]	14	56	103	75 ± 12 [2]	73

[1] Statistically significant differences according to the Mann–Whitney U test. [2] Statistically significant differences according to the Wilcoxon test.

3.3.1. Absolute Mean Deviation

The precision based on absolute mean deviation values was 74 μm (SD ± 22 μm) for [CON]; 32 μm (SD ± 10 μm) for [PRINT] and 15 μm (SD ± 4 μm) for [IOS]. The comparisons of [CON] and [PRINT] and of [IOS] and [PRINT] showed statistically significant differences.

3.3.2. Root Mean Square Error

The precision based on RMSE values was 130 μm (SD ± 26 μm) for [CON], 66 μm (SD ± 12 μm) for [PRINT] and 75 μm (SD ± 12 μm) for [IOS]. The comparisons of [CON] and [PRINT] and of [IOS] and [PRINT] showed statistically significant differences.

3.3.3. Atos Scans

The precision of the five ATOS scans was 2 μm (SD ± 1 μm).

4. Discussion

In the present study, the absolute mean deviations of the [REF]-[PRINT] revealed significantly better results compared with [REF]-[CON]. Therefore, the null hypothesis had to be rejected for the full-arch values.

In the present study, the absolute mean deviation was 69 μm (SD ± 24 μm) and the RMSE was 119 μm (SD ± 29 μm) for the conventional workflow represented by gypsum casts. Since the deviations are squared in RMSE, high outliers were considered with a higher impact. Other studies revealed absolute mean deviations around 16.2 μm (SD ± 14.5 μm) and 15 μm (SD ± 4 μm) [21,22]. Absolute median values of 16.3 μm (SD ± 2.8 μm) and an RMSE of 28.49 μm (SD ± 1.74 μm) were reported [1,23]. One explanation for the higher deviation values observed in the present study may be that the reference model exhibited pronounced interdental undercuts. Schlenz et al. stated that interdental areas in periodontally compromised dentitions are better displayed in intraoral scans than conventionally [24]. Furthermore, the crown lengths might exceed the heights of the crowns used in other studies. The anterior segment was relatively protruded. Although massive undercuts were partially blocked with wax, these properties may have resulted in higher withdrawal forces when removing the impression trays. As a result, there was a risk of deformation of the impression material. In that case, this phenomenon should have happened unnoticed since the quality of the impression was checked thoroughly to detect visible defects and to ensure a stable connection to the tray. In comparable studies, polyvinyl siloxane was used as established conventional impression material [1,21,25]. The study setup was tested thoroughly to get used to the material and to check the test environment. Before the main experiment was performed the workflow was tested by thirty impressions. The manufacturer's instructions were kept in all aspects for impression taking and further processing.

The full-arch accuracy of the conventional workflow [REF]-[CON] and of the digital printer workflow [REF]-[PRINT] was evaluated by surface deviation measurement [23,26].

To avoid unnecessary outliers during registration and deviation measurements, the digital data sets and the reference data set were identically trimmed at the borders and at the proximal areas. Additionally, all outlier measurements >2.00 mm were discarded before the calculation of deviations to avoid the inclusion of obvious artifacts. In other studies, the 20/80 quantile, the 10/90 percentile, and the 5/95 quantile were used due to the assumption that values beyond these thresholds were irrelevant artifacts [17,23,26,27]. In the present study, 1/99, 5/95, and 10/90 ranges would have excluded relevant values (Figure 4).
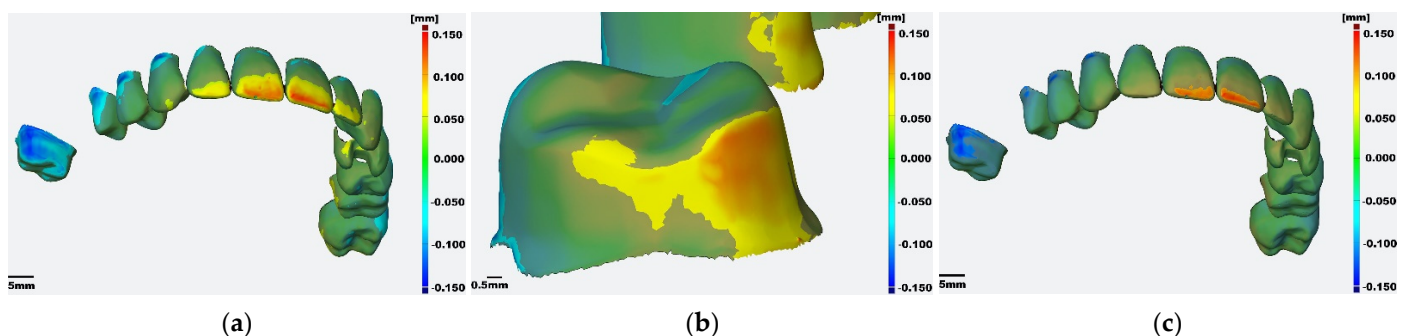

Figure 4. Excluded areas depending on the included quantiles [Scale ± 150 μm]: (**a**) 10/90 quantile (highlighted area = excluded); (**b**) 5/95 quantile (highlighted area = excluded); (**c**) 1/99 (highlighted area = excluded).

According to the authors' knowledge, this was the first study that evaluated the digital workflow by comparing the different steps with each other. The first step within the digital workflow was to achieve a digital data set from the reference cast using an intraoral scanner. The full-arch mean trueness value of these scans [REF]-[IOS] was 19 μm (SD ± 3 μm). The

precision based on absolute mean deviation was 15 μm (SD ± 4 μm). A study of the same working group found a full-arch accuracy of 29 μm (SD ± 3 μm) using the same intraoral scanner but with an older software version (v5.1) [26]. In the former study, machined zirconia tooth surfaces were captured. To imitate tooth-like optical properties, the teeth of the present study were made of lithium disilicate with glazed surfaces. Only the prepared surfaces were left as machined. These optical properties were important to provide realistic optical conditions for the optical impression system.

Dutton et al. described that highly translucent materials can affect the accuracy [28]. They stated that materials such as lithium disilicate can decrease trueness and precision [28]. For Primescan, scanning lithium disilicate with a medium translucency and a Vita color A2 showed the highest mean deviation for both trueness (23 μm ± 3 μm) and precision (33 μm ± 4 μm) compared to fourteen other groups (e.g., composites, metals, dentin, enamel, etc.) [28]. The lowest mean deviation was obtained for polished amalgam with a trueness of 11 μm and a precision of 16 μm [28]. Due to the small differences between the lowest and highest trueness values, the influence of the material properties must be relativized. Although glazed lithium disilicate teeth were used in this study, the scans showed a good accuracy.

Other authors using the same type of scanner based on the principle of parallel confocal microscopy achieved a full-arch trueness of about 30 μm [23,29]. Ender et al. obtained trueness values of 33.9 μm (SD ± 7.8 μm) for the (90-10)/2 percentile [23]. Schmidt et al. found mean deviation values of 33.8 μm (SD ± 31.5 μm) [29]. However, all authors used software versions, which were below the version which was used in the present study (v5.2.2 RC1).

Local mean trueness values of [local_IOS] ranged from 7 μm (SD ± 6 μm) to 11 μm (SD ± 2 μm). RMSE values were between 9 μm (SD ± 7 μm) and 15 μm (SD ± 4 μm). These minor differences between absolute mean deviation and RMSE values underlined the small spread of the deviation values. Zimmermann et al. reported a local accuracy of 18.7 μm (SD ± 2.8 μm) using the (95-5)/2 percentile [27].

Within the digital workflow, the digital data sets which were produced with the intraoral scanner [IOS] were transferred into real casts by DLP printing. For evaluating the accuracy of the printer, this step is decisive. The lower the deviation between the digital data set and the corresponding cast the better the accuracy of the printer. This aspect was evaluated in the present study by digitizing the printed casts with an industrial scanner and comparing these data sets [PRINT] with their corresponding digital data sets obtained from the intraoral scanner [IOS]. The absolute mean deviation in this working step was 38 μm. The standard deviation was 6 μm, the range of deviation values was between 28 μm (minimum) and 49 μm (maximum), the median value was 38 μm, and the root mean square error was 58 μm. In particular, the latter value indicates the low variation of the printed objects.

For clinical relevance, the deviation of the printed object from the original situation is of major importance. Full-arch accuracy is essential for the fitting process of CAD/CAM generated prosthetic restorations to assess occlusal contacts and dynamic contacts in articulated casts. Full-arch accuracy is also important to check proximal contacts of dental restorations or for the manual veneering of metal-based or ceramic frameworks. Local accuracy focuses on the preparation itself, neglecting adjacent teeth; therefore, the significance of proximal contacts is not considered. For fitting of multi-unit fixed partial dentures, full-arch accuracy is mandatory, too. Furthermore, the full-arch accuracy analysis is necessary to define overall distortions. In the present workflow, the digital workflow showed an absolute mean trueness of 33 μm (SD ± 4 μm) and an RMSE trueness of 48 μm (SD ± 6 μm). Other studies reported a mean trueness deviation of 97 μm (SD ± 73 μm) and RMSE values of 105.5 μm (SD ± 22,5 μm), 27 μm (SD ± 7 μm) and 28.09 (SD ± 2.11 μm) [1,30–32]. For SLA, Choi et al. showed RMSE values of 85.2 μm (SD ± 13.1 μm) [32]. Park et al. reported median trueness values of 146.6 μm for FFF and 125.2 for photopolymer jetting [33]. CLIP was shown in recent literature with a trueness of 48 μm (SD ± 44 μm) [30].

The full-arch precision results based on mean deviation of 32 μm (SD ± 10 μm) were competitive, too. Choi et al. stated a precision of 53.8 μm (SD ± 22.5 μm) [32].

The analysis of the single steps, [REF]-[IOS], [IOS]-[PRINT], and [REF]-[PRINT], revealed that the widening of the arch in the molar area, whilst performing intraoral scans, was partially compensated by a relative compression of the arch by the printing process. Figure 5 shows this observation exemplarily. On the condition that the deviations in the different working steps took place in the same area which was confirmed by the color maps, the compensation theory can be justified as follows: [REF]-[IOS] showed an absolute mean deviation of 19 μm. Based on the intraoral scan, [IOS]-[PRINT] differed by 38 μm. For [REF]-[PRINT], deviations in the same direction resulted in the sum of [REF]-[IOS] and [IOS]-[PRINT] (19 μm + 38 μm). In this study, [REF]-[PRINT] displayed an absolute mean deviation value of 33 μm which was below the sum value (19 μm + 38 μm) and additionally below the deviations of [IOS]-[PRINT]. This indicates that the deviations acted in opposite directions (widening and compression) and consequently compensated each other. The compression after printing can be explained by a potential shrinkage of the printed object during polymerization.
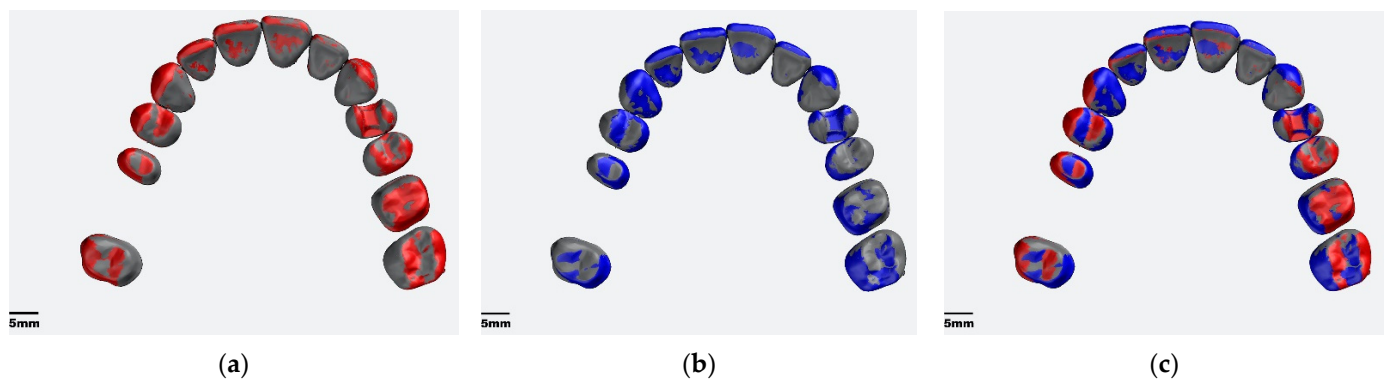

(**a**)　　　　　　　　　　　　(**b**)　　　　　　　　　　　　(**c**)

Figure 5. Compensation of the arch widening during the entire workflow: (**a**) [REF]-[IOS] (grey = REF; red = IOS). In the [IOS], the arch is widened in relation to the reference cast; (**b**) [REF]-[PRINT] (grey = ref; blue = printed). The printed cast exhibits a narrower arch than the original; (**c**) superimposition [REF]-[IOS] and [REF]-[PRINT]. The "widening" by the intraoral scan is overcompensated by the printed cast.

The local RMSE deviations of [local_PRINT] were 35 μm (SD ± 9 μm) for the FDP preparation, 18 μm (SD ± 5 μm) for the single crown, and 19 μm (SD ± 3 μm) for the inlay preparation. Other authors using a DLP printer achieved RMSE trueness values of 51.39 μm (SD ± 3.37 μm) for FDP preparations, 46.93 μm (SD ± 2.28 μm) for crown preparations, and 46.0 μm (SD ± 1.58 μm) for inlay preparations [1]. Choi et al. described RMSE values of 66.9 (SD ± 20.9) for inlays, 84.3 (SD ± 22.5) for single crowns, and 117.3 μm (SD ± 38.5) for FDP [32]. Therefore, the results of the present study were comparable or lower than the findings in recent literature. Trueness RMSE values reported for SLA were 60.7 μm (SD ± 12.1 μm) for inlays, 62.0 μm (SD ± 10.6 μm) for single crowns, and 81.5 μm (SD ± 14.1 μm) for FDP [32]. Cho et al. reported RMSE values of 22 (SD ± 5) for the internal area [31].

The local accuracy values of the FDP preparation obtained from [local_CON] and from [local_PRINT] did not differ significantly, whereas the values of the inlay preparation and the single crown preparation of the [local_PRINT] were more than twice lower than the [local_CON] trueness. In the case of the inlay and crown preparation, the standard deviations for [local_CON] were more than five times higher than those for [local_PRINT]. The RMSE values amplified these observations. The high [local_CON] trueness values of the inlay and single crown preparation could be explained by high retention forces that were necessary when removing the impression from the reference cast. These applied high forces may have led to an irreversible distortion of the polyvinyl siloxane. It could be

retraced that the removal of the impression tray was always started at the location of the first left molar so that the highest forces might have been applied in this area.

The absolute mean trueness full-arch values of [REF]-[CON] were almost twice as high as the deviations [local_CON] for the FPD preparation and the inlay preparation. The absolute mean value for [local_PRINT$_{17-15}$] showed 26 μm and differed only slightly from the full-arch trueness of [REF]-[PRINT] exhibiting 33 μm. The [local_PRINT$_{24}$] and [local_PRINT$_{26}$] trueness showed identical values independently from the type of preparation which were half of the full-arch trueness values of [REF]-[PRINT]. Thus, the differences in geometry between an internal (inlay) and circular (crown) preparation had no influence on trueness.

5. Conclusions

Within the limits of this study, the following conclusions were drawn:

The printed casts obtained from a DLP printer revealed significantly better full-arch trueness and precision results compared to conventionally fabricated casts.

With respect to full-arch trueness, the widening of the arch in the molar area of the intraoral scan was overcompensated by the compression of the cast in the same area during the printing process.

With respect to local trueness, the low deviation values of printed casts were comparable to the local trueness results of IOS reported in the literature. The local trueness of inlay and crown preparations suggested the adequate usability of printed casts for checking the marginal fit of inlay and crown restorations. The full-arch and the local trueness of the FDP showed the usability for checking proximal and occlusal contacts of CAD/CAM fabricated restoration or for veneering purposes.

References

1. Sim, J.Y.; Jang, Y.; Kim, W.C.; Kim, H.Y.; Lee, D.H.; Kim, J.H. Comparing the accuracy (trueness and precision) of models of fixed dental prostheses fabricated by digital and conventional workflows. *J. Prosthodont. Res.* **2019**, *63*, 25–30. [CrossRef] [PubMed]
2. Etemad-Shahidi, Y.; Qallandar, O.B.; Evenden, J.; Alifui-Segbaya, F.; Ahmed, K.E. Accuracy of 3-Dimensionally Printed Full-Arch Dental Models: A Systematic Review. *J. Clin. Med.* **2020**, *9*, 3357. [CrossRef] [PubMed]
3. Zimmermann, M.; Mehl, A.; Rosentritt, M.; Ilie, N.; Lohbauer, U. Dentale CAD/CAM-Technologie. In *Werkstoffkunde in der Zahnmedizin 1. Auflage*; Thieme: Stuttgart, Germany, 2018. [CrossRef]
4. Revilla-Leon, M.; Ozcan, M. Additive Manufacturing Technologies Used for Processing Polymers: Current Status and Potential Application in Prosthetic Dentistry. *J. Prosthodont.* **2019**, *28*, 146–158. [CrossRef] [PubMed]

5. Ligon, S.C.; Liska, R.; Stampfl, J.; Gurr, M.; Mulhaupt, R. Polymers for 3D Printing and Customized Additive Manufacturing. *Chem. Rev.* **2017**, *117*, 10212–10290. [CrossRef] [PubMed]

6. Alifui-Segbaya, F. Biomedical photopolymers in 3D printing. *Rapid Prototyp. J.* **2019**, *26*, 437–444. [CrossRef]

7. Stansbury, J.W.; Idacavage, M.J. 3D printing with polymers: Challenges among expanding options and opportunities. *Dent. Mater.* **2016**, *32*, 54–64. [CrossRef]

8. Methani, M.M.; Revilla-Leon, M.; Zandinejad, A. The potential of additive manufacturing technologies and their processing parameters for the fabrication of all-ceramic crowns: A review. *J. Esthet. Restor. Dent.* **2019**, *32*, 182–192. [CrossRef]

9. Pillai, S.; Upadhyay, A.; Khayambashi, P.; Farooq, I.; Sabri, H.; Tarar, M.; Lee, K.T.; Harb, I.; Zhou, S.; Wang, Y.; et al. Dental 3D-Printing: Transferring Art from the Laboratories to the Clinics. *Polymers* **2021**, *13*, 157. [CrossRef]

10. Revilla-Leon, M.; Sadeghpour, M.; Ozcan, M. An update on applications of 3D printing technologies used for processing polymers used in implant dentistry. *Odontology* **2020**, *108*, 331–338. [CrossRef]

11. Kasparova, M.; Grafova, L.; Dvorak, P.; Dostalova, T.; Prochazka, A.; Eliasova, H.; Prusa, J.; Kakawand, S. Possibility of reconstruction of dental plaster cast from 3D digital study models. *Biomed. Eng. Online* **2013**, *12*, 49. [CrossRef]

12. Ellakany, P.; Al-Harbi, F.; El Tantawi, M.; Mohsen, C. Evaluation of the accuracy of digital and 3D-printed casts compared with conventional stone casts. *J. Prosthet. Dent.* **2020**. [CrossRef] [PubMed]

13. Wenbin, H.; Tsui, L.; Haiging, G. A study of the staircase effect induced by material shrinkage in rapid prototyping. *Rapid Prototyp. J.* **2005**, *11*, 82–89. [CrossRef]

14. Zhou, J.G.; Herscovici, D.; Chen, C.C. Parametric process optimization to improve the accuracy of rapid prototyped stereolithography parts. *Int. J. Mach. Tools Manuf.* **2000**, *40*, 363–379. [CrossRef]

15. Shuaib, M.; Haleem, A.; Kumar, S.; Javaid, M. Impact of 3D printing on the environment: A literature-based study. *Sustain. Oper. Comput.* **2021**, *2*, 57–63. [CrossRef]

16. Hui, J.; Ding, K.; Chan, F. An investigation on energy consumption and part quality of stereolithography apparatus manufactured parts. *Rapid Prototyp. J.* **2022**, *28*, 52–67. [CrossRef]

17. Mehl, A.; Reich, S.; Beuer, F.; Güth, J.F. Accuracy, trueness, and precision—A guideline for evaluation of these basic values in digital dentistry. *Int. J. Comput. Dent.* **2021**, *24*, 341–352.

18. Passos, L.; Meiga, S.; Brigagao, V.; Street, A. Impact of different scanning strategies on the accuracy of two current intraoral scanning systems in complete-arch impressions: An in vitro study. *Int. J. Comput. Dent.* **2019**, *22*, 307–319.

19. Dold, P.; Bone, M.C.; Flohr, M.; Preuss, R.; Joyce, T.J.; Deehan, D.; Holland, J. Validation of an optical system to measure acetabular shell deformation in cadavers. *Proc. Inst. Mech. Eng. H* **2014**, *228*, 781–786. [CrossRef]

20. Yatmaz, B.; Raith, S.; Reich, S. Trueness evaluation of digital impression: The impact of the selection of reference and test object. *J. Dent.* **2021**, *111*, 103706. [CrossRef]

21. Bohner, L.; Hanisch, M.; De Luca Canto, G.; Mukai, E.; Sesma, N.; Neto, P.T. Accuracy of Casts Fabricated by Digital and Conventional Implant Impressions. *J. Oral. Implantol.* **2019**, *45*, 94–99. [CrossRef]

22. Kuhr, F.; Schmidt, A.; Rehmann, P.; Wostmann, B. A new method for assessing the accuracy of full arch impressions in patients. *J. Dent.* **2016**, *55*, 68–74. [CrossRef] [PubMed]

23. Ender, A.; Zimmermann, M.; Mehl, A. Accuracy of complete- and partial-arch impressions of actual intraoral scanning systems in vitro. *Int. J. Comput. Dent.* **2019**, *22*, 11–19. [PubMed]

24. Schlenz, M.A.; Schubert, V.; Schmidt, A.; Wostmann, B.; Ruf, S.; Klaus, K. Digital versus Conventional Impression Taking Focusing on Interdental Areas: A Clinical Trial. *Int. J. Environ. Res. Public Health* **2020**, *17*, 4725. [CrossRef] [PubMed]

25. Al-Imam, H.; Gram, M.; Benetti, A.R.; Gotfredsen, K. Accuracy of stereolithography additive casts used in a digital workflow. *J. Prosthet. Dent.* **2018**, *119*, 580–585. [CrossRef] [PubMed]

26. Reich, S.; Yatmaz, B.; Raith, S. Do "cut out-rescan" procedures have an impact on the accuracy of intraoral digital scans? *J. Prosthet. Dent.* **2020**, *125*, 89–94. [CrossRef]

27. Zimmermann, M.; Ender, A.; Mehl, A. Local accuracy of actual intraoral scanning systems for single-tooth preparations in vitro. *J. Am. Dent. Assoc.* **2020**, *151*, 127–135. [CrossRef]

28. Dutton, E.; Ludlow, M.; Mennito, A.; Kelly, A.; Evans, Z.; Culp, A.; Kessler, R.; Renne, W. The effect different substrates have on the trueness and precision of eight different intraoral scanners. *J. Esthet. Restor. Dent.* **2020**, *32*, 204–218. [CrossRef]

29. Schmidt, A.; Klussmann, L.; Wostmann, B.; Schlenz, M.A. Accuracy of Digital and Conventional Full-Arch Impressions in Patients: An Update. *J. Clin. Med.* **2020**, *9*, 688. [CrossRef]

30. Rungrojwittayakul, O.; Kan, J.Y.; Shiozaki, K.; Swamidass, R.S.; Goodacre, B.J.; Goodacre, C.J.; Lozada, J.L. Accuracy of 3D Printed Models Created by Two Technologies of Printers with Different Designs of Model Base. *J. Prosthodont.* **2020**, *29*, 124–128. [CrossRef]

31. Cho, S.H.; Schaefer, O.; Thompson, G.A.; Guentsch, A. Comparison of accuracy and reproducibility of casts made by digital and conventional methods. *J. Prosthet. Dent.* **2015**, *113*, 310–315. [CrossRef]

32. Choi, J.W.; Ahn, J.J.; Son, K.; Huh, J.B. Three-Dimensional Evaluation on Accuracy of Conventional and Milled Gypsum Models and 3D Printed Photopolymer Models. *Materials* **2019**, *12*, 3499. [CrossRef] [PubMed]

33. Park, M.E.; Shin, S.Y. Three-dimensional comparative study on the accuracy and reproducibility of dental casts fabricated by 3D printers. *J. Prosthet. Dent.* **2018**, *119*, 861.E1–861.E7. [CrossRef] [PubMed]